LCL filter Design and Current Control of Grid Interfaced Voltage Source Inverter

Sajad Sarajian[*][1]

[1] Department of Electrical Engineering, Islamic Azad University, Ashtian Branch,
Ashtian, Iran

Oct 7, 2014

Abstract

This paper deals with design and implementation of a grid interfaced voltage source converter which uses an LCL passive filter in its output terminal and a Proportional Resonance (PR) controller to delivering power of a distributed generation source to power utility and local load. LCL filer in output of the converter analytically is designed and its different transfer functions are obtained for assessment on elimination of any probable parallel resonant in power system. The power converter uses a controller system to work on two modes of operation, stand-alone and grid-connected modes, and also has a seamless transfer between these two modes of operation. Furthermore, a fast semiconductor-based protection system is designed for the power converter. Performance of the designed grid interface converter is evaluated by using an 85 kVA industrial setup.

Keywords: Proportional-resonant controller, voltage source inverter, grid-interfaced converter, filters design, and renewable energy sources.

1 Introduction

Distributed Generation (DG) systems such as microturbines, fuel cells, wind turbines and photovoltaic systems are expected to represent a large portion of power generation capacity, especially in future [1]. In particular, Micro Turbine Generator (MTG) is witnessed to be capable of delivering clean energy from a wide variety of fuels with superior safety and low emissions [2-3]. The capacity of MTG can be ranged from several kilowatts up to megawatts. As it is often sited dispersedly near the industrial load, it is deemed as a category of distributed generations nowadays [4–5]. A direct merit exhibited by such electric power generation is to provide the utility a way to defer power plant construction, while offering customers a clean resource at reasonable cost.

There are essentially two types of micro turbine designs. One is a split shaft design that uses a power turbine rotating at 3600 rpm and a conventional generator (usually induction generator) connected via a gearbox. The power inverters are not needed in this design. Another is a high-speed single-shaft design with the compressor and turbine mounted on the same shaft as the Permanent Magnet (PM) synchronous generator. The advantages of the high-speed permanent-magnet generator are its compact size, low-mass design and the elimination of the gearbox, resulting in reduction and simplification of the generating package. The use of power electronics enhances the system performance because of the asynchronous operation of the gas turbine, with the gas turbine speed independent of the grid frequency. It enables the gas turbine speed control to adjust for optimal gas turbine efficiency [6-7].

---

[*] sajadsarajian@yahoo.com

A general view of microturbine system is shown in Fig. 1. The configuration of an MTG system is composed of a gas turbine, a compressor, and an AC generator. They are inertia welded on a single shaft to simplify the mechanical structure. When this shaft turns at the speed of the turbine, the generator would provide high-frequency AC electricity that requires a rectifier (Converter 1 in Fig. 1) and an inverter (Converter 2 in Fig. 1) to interface with utility network. By employing different control strategies, the MTG can operate as a power conditioner for the grid-connected operation to improve the quality of supplying power or sever from the grid as an emergency generator [8-9].
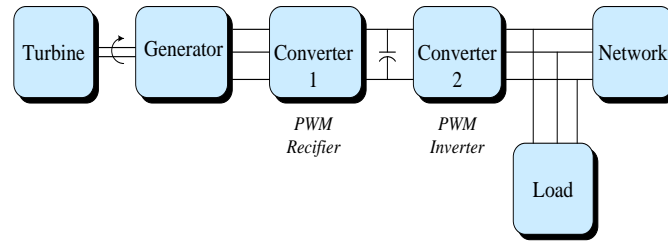

Figure 1: Block diagram of power electronic interface configuration for a MT.

The grid-connected inverter in MT's power electronic interface should operate in grid-tied and off-grid modes in order to provide power to the emergency load during system outages. Moreover, the transition between the two modes should be seamless to minimize any sudden voltage change across the emergency load or any sudden current change to the grid. A seamless transfer between both modes has been proposed in [10-12]. However, the grid current controller and the output voltage controller must be switched between the two modes, so the outputs of both controllers may not be equal during the transfer instant, which will cause the current or voltage spikes during the switching process. On the other hand, as the grid-interactive inverter should operate in off-grid mode, the filter capacitor is necessary. Nevertheless, the filter capacitor current affects the waveform quality of the grid current in polluted grid, especially at low output power [13-16].

This paper deals with design and construction of a three-phase 85 kVA grid-interactive inverter and its Digital Signal Processor (DSP)-based digital controller. Two different control modes are considered for the inverter: stand-alone control mode, and grid-connected control mode. Furthermore the inverter controller is expected to have a soft and seamless transfer between these two control modes. In the following sections, first the overall configuration of system is discussed in section 2, and then in section 3, the controller of inverter is described; a protection system proper for the power inverter is presented in section 4; in sections 5 and 6 design procedure for inverter output LCL filter and digital controller implementation are explained, respectively. Section 7 shows the experimental results of the implemented inverter; paper's conclusion is also presented in section 8.

2   Three-Phase Grid Interactive Inverter

Power configuration of the developed system is depicted in Fig. 2. It consists of a primary power source, a full bridge diode rectifier, a DC-link, a full bridge grid converter with LC filter, a power electromechanical relay *K*, and the three-phase 400 V/ 50Hz grid. The primary power source is, in fact, a microturbine generator that in this study is replaced with a grid connected power autotransformer. The parameters used in the constructed system are shown in Table 1.
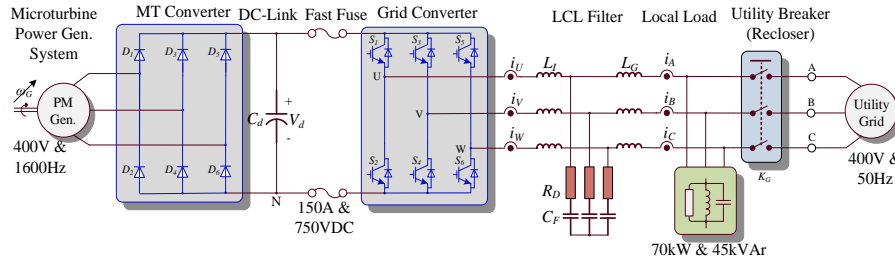
Figure 2: General configuration of constructed grid-tied inverter.

3   Digital Controller of Inverter

A control technique should be designed for inverter (750 Vdc/ 400 Vac (L-L), rated 70 kW) to satisfy following performance characteristics:

1. *Low load regulation (less than 5%):* the AC output voltage of the DG system should be maintained at 400 V (L-L)/230 V (L-N) independent of load conditions,
2. *Minimum Total Harmonic Distortion (THD):* DG system when feeding to the nonlinear loads, such as rectifiers, Switched Mode Power Supplies (SMPS), must generate minimum harmonics currents and voltages in compliant with IEEE 519 std,
3. *Fast transient response:* system must be able to produce output AC voltage with minimum overshoot or undershoot,

Table 1: System Parameters

Parameter	Value
System voltage: V_{L-L} (= V_b)	400 V$_{rms}$
Fundamental frequency: f_{Line}	50 Hz
Load rated: P_n, Q_n, S_n (= S_b)	70 kW, 45 kVAr, 85 kVA
DC link voltage: V_{dc}	760 Vdc (1.9 p.u.)
DC-link Capacitor: C_{dc}	4200 μF
Switching Frequency	2 kHz (40 p.u.)
Sampling Frequency	4 kHz (80 p.u.)
PI controller	K_P = 0.5, K_I = 200
Load Power Factor	0.85
System impedance parameters: L_S, R_S	55μH, 2.5 mΩ
LCL filter parameters:	
L_1, R_1	0.83 mH (13.85%), 52 mΩ
L_2, R_2	0.75 mH (12.52%), 12 mΩ
C_F	270 μF (15.97%)
R_d	0.6 Ω (31.88%)
f_{res}	488 Hz (976%)

4. *Short circuit protection:* system must be able to provide protection from excessive overload conditions,
5. *Different control modes:* the microturbine grid converter should operate in both grid-connected control mode and stand-alone control mode,
6. *A soft and seamless transfer between different control modes:* in transition from one control mode to the other, amplitude and frequency of the voltage at the PCC must not exit its limitation ($V_{rated} \pm 10\%$ & $f \pm 2$ Hz),
7. *Anti-islanding detection capability:* based on IEEE 1547 std [17], all DGs must be disconnected from an islanded grid in a specified time,
8. *Paralleling capability:* in order to increase the reliability of power source converter, it should operate in parallel with other converters, especially in stand-alone operation mode,

9. *Deals with distorted and/or unbalanced grid voltage:* grid voltage is commonly distorted and/or unbalanced. Therefore, it causes grid-tied inverters to inject a distorted and/or unbalanced current to the power system. So, inverter's controller must be able to suppress these harmonic effects.
10. *Decupled P & Q control for grid-connected inverter:* in grid-connected control mode the control of the active and reactive power must be decoupled from each other.

3.1   Island Mode Operation

One of the most uses of microturbine system is in places that are far from electric utility power system. In this case, this device should produce a power appropriate for local load which is supplied by microturbine system. Therefore, system must be controlled in such a way that reference voltage appears in output terminal and delivers power to the local loads [18].

In stand-alone control mode, no grid exists so the output voltages need to be controlled in terms of amplitude and frequency and thus the reactive and, respectively, active power flow is controlled [19]. In the case of unbalance between the microturbine generated and the load required power, adjustment of the speed of the microturbine can regulate the produced power in a limited range. The potential excess of power will be quickly dissipated in a damp resistor by starting a chopper control located in DC-link of inverter (it does not show in Figure 2).

One of the common control methods of inverter, in this case, is control of output voltage in *dq* plan. The control structure for stand-alone control mode is shown in Figure 3 and it consists of output voltage controller, and current limiter. The output voltage controller is aiming to control the output voltage with a minimal influence from the shape of the nonlinear load currents or load transients. A standard Proportional Integrate (PI) controller operating in the synchronously rotating coordinate system where is kept to zero is used. As it can be seen form Figure 3, at first, the output voltages are measured (by voltage sensors) and after converting to V_d and V_q, they are subtracted from their references, and the resultant error signals send to two separate PI controllers; PI controllers produce the pattern voltages for switching in *dq* plan. Then, these voltages are converted to the pattern voltage in *abc* plan and introduce to PWM generating block. Finally, the PWM generating block generates six PWM pulses for Insulated Gate Bipolar Transistor (IGBT) switches in inverter.
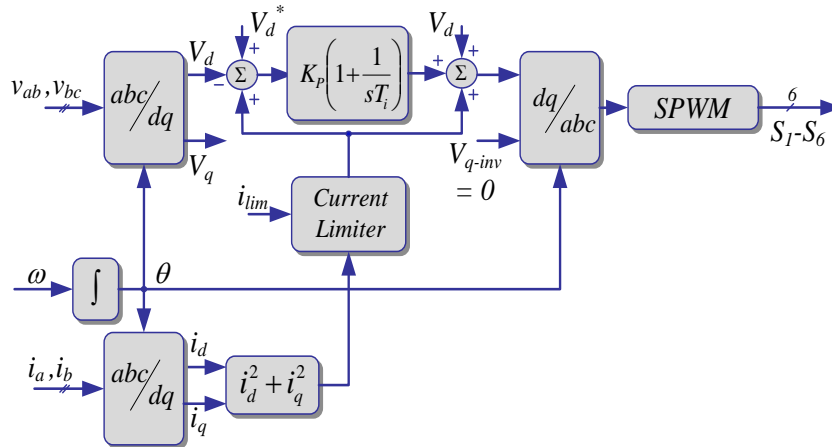

Figure 3: Block diagram of stand-alone control of inverter.

When the load current exceeds the rated current, the current limiter will decrease the output voltage reference in the allowed range, and for fast response there is a direct forward connection to the voltage controller output. This situation can occur if at a certain load, the generated power decreases due to lower microturbine input fuel or during overloading.

3.2 Grid-Tied Mode Operation

In grid-connected control mode, principally all the available power that can be obtained from the microturbine is delivered to the grid. Moreover, compensation of reactive power is possible if required. Typically, the inner current loop is implemented using a stationary PI current controller with voltage feedforward, as shown in Fig. 4(a). Using PI control, however, leads to steady-state current error (both in phase and magnitude) when tracking sinusoidal input, and hence a poor harmonic compensation performance is expected [9]. Instead, the equivalent stationary PR controller can be used as the inner current controller, as shown in Fig. 4(b).Compared to a stationary PI controller, the only computational requirement imposed by the PR controller is an extra integrator for implementing a second-order system, but with a modern low-cost 32-bit fixed/floating-point DSP, this increase in computation can generally be ignored [9]. Besides that, using a PR controller would allow the removal of the grid voltage feedforward path, as proven in [9], and the simple cascading of a HC compensator for eliminating selected low-order harmonics.
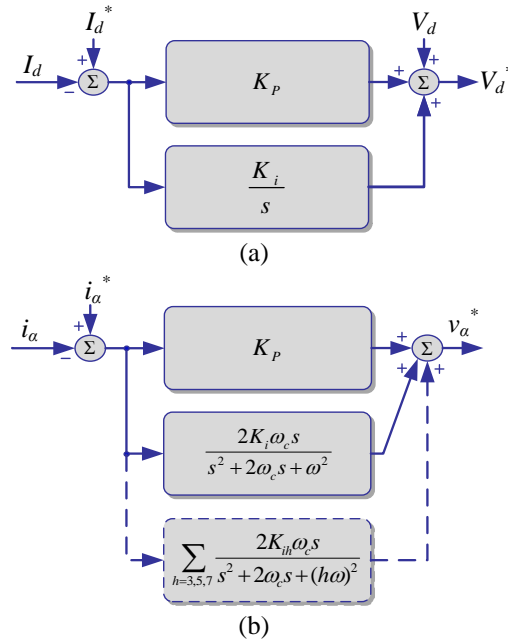

Figure 4: Single-phase grid inverter control, (a) Stationary PI control, (b) Stationary PR inner current control

Three-phase control in the stationary α–β frame can be viewed as two independent control paths along the α and β axes, respectively. For illustration, Fig. 5 shows the inner current control scheme of a three-phase grid-tied inverter, where a second PR controller is added, as compared to that in Fig. 4(b). In the conventional synchronous PI method, multiple frame transformations and control decoupling are needed. These complications are obviously removed from Fig. 5 when PR controllers are used instead.
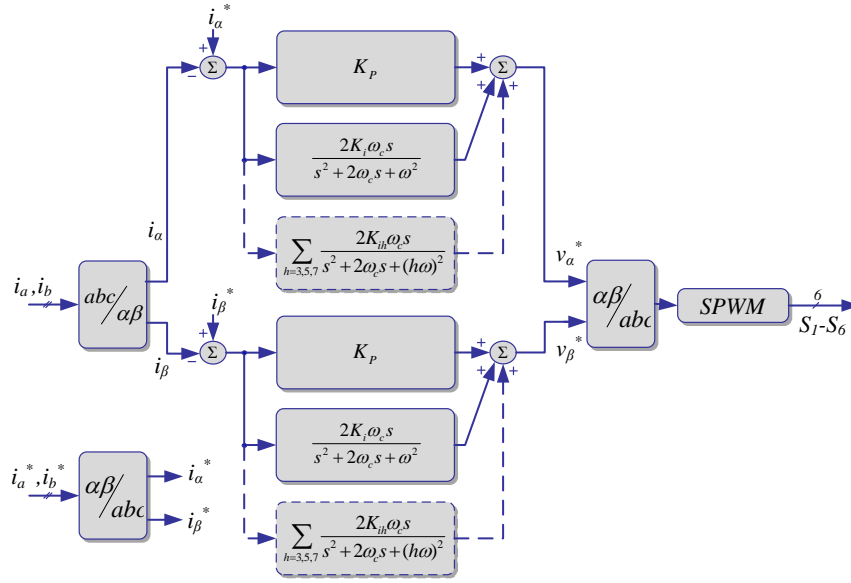
Figure 5: Three-phase grid inverter current control, using PR controllers

3.3 Seamless Transfer

In order to realize the seamless transfer between grid-tied and off-grid modes, the load voltage must match the magnitude, frequency, and phase of the grid voltage well before connecting to the utility. The load voltage can match the grid voltage well through sampling the grid voltage as the reference voltage before connecting to the grid, especially in polluted grid voltage. The detailed process of the seamless transfer between the two modes is illustrated in the following.

1. **Off-grid mode to grid-tied mode:**

   o   Detect that the grid is normally operating.
   o   Adjust the inverter's output voltage (or load voltage) to match the magnitude and phase of the grid voltage.
   o   Once the load voltage is equal to the grid voltage, turn on the relay *K* and switch inverter from voltage-controlled mode to current-controlled mode, with the reference current being equal to the load current.
   o   Change the reference current slowly to the desired current (both magnitude and phase).

2. **Grid-tied mode to off-grid mode:**

   o   Detect a fault on the grid and give a turn off signal to the relay *K*.
   o   Monitor the magnitude and phase of the load voltage.
   o   When the relay current goes to zero, transit the inverter to a voltage-controlled mode, with the voltage reference being derived from the load voltage.
   o   Ramp up the magnitude of the load voltage from its initial value to the rated value.

4 Power Converter's Protection System

Electrical faults, that can damage the power converter, are categorized in two groups: overvoltage and over-current. Each one of these faults has different severe effects on the system, so an effective protection method should be used.

4.1 Over Current

Many reasons may cause an over-current occurrence in a power inverter. Overload and short-circuit are the main and common reasons of over-current fault in a power inverter. Overload fault lasts in a longer time (e.g. 1 min.) and current value is a few times of nominal current (e.g. 1-2 p.u). The delayed function fuses are used to protect system against this fault, while short circuit lasts for a short time (e.g. 10 µs to 1 ms) and current increases several times beyond rating current (e.g. 2-100 p.u.). As a result, the short-circuit fault is more severe than over-current and therefore needs a faster protection system.

Over current is the most common fault; it is implemented in both software and hardware. Semiconductor fuses and gate driver protection are used as hardware methods.

Phase to phase short circuit on inverter AC side (i.e. Figure 6(a)) makes the biggest current flowing in IGBT switches; due to AC side filter inductors; current increasing rate is not too fast, as a result, both common software and hardware methods can do effective protection in this case.
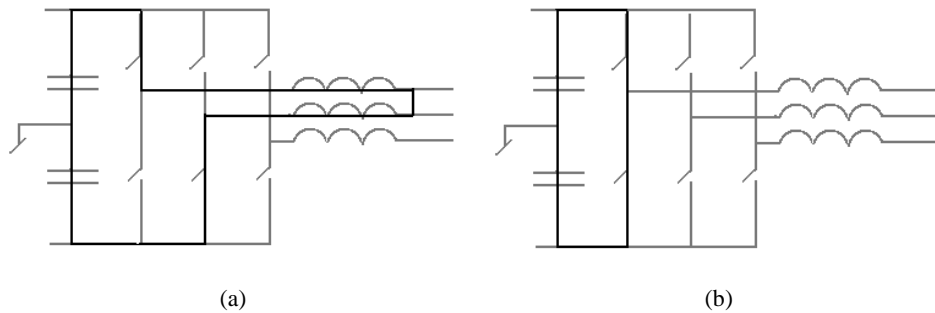

(a)   (b)

Figure 6: Over current faults (a) shout through (b) AC side short circuit.

Shout through at dc link (i.e. Figure 6(b)) is another severe fault; it should note that shout through is not expected to happen after completing the control system and required protections; however if this fault happens, effective protection is not possible either by software or hardware. A brief analysis regarding shout through and AC side short circuit is explained as follows.
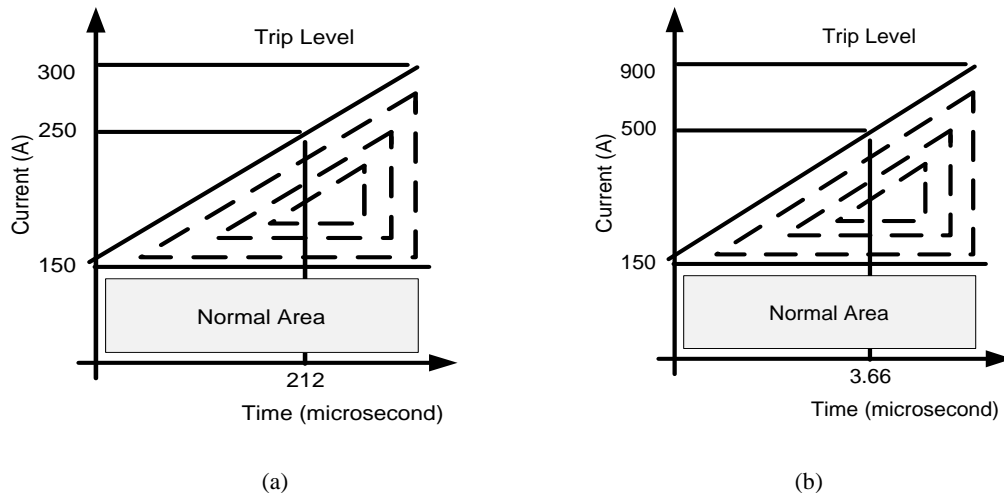

(a)   (b)

Figure 7: Over current Protection criteria (a) inverter AC side (b) DC-Link.

Considering 2 µH leakage inductance in DC-link at experimental setup and 800 µH filter inductance at inverter AC side; current rising rate due to short circuit at dc link and AC side are 375 and 0.47 A/µS, respectively. It should note that DC-link voltage at steady state is 750 V, subsequently current rise rate is as:

$$\frac{di}{dt} = \frac{V(V)}{L_\sigma(\mu H)} \quad \frac{A}{\mu S} \tag{1}$$

Where L_σ is the leakage inductance and V is the DC-link voltage. Finally, protection areas in DC-link and inverter AC side are shown in Figures 7(a) and (b), respectively. Shaded areas demonstrate the protection system setting points.

In the constructed inverter, following protection systems are considered to protect it against any probable over-current or short-circuit faults:

1. *A software-based protection system implemented by DSP digital controller:* it can clear the fault in less than 120 μs,
2. *Fast semiconductor fuses:* they are installed in DC-link and AC terminals of power inverter,
3. *A circuit breaker:* installed in output terminal of inverter after the *LC* filter and before connecting to the grid or local load,
4. *Short-circuit protection system of Intelligent Power Module (IPM):* IPMs are commonly equipped by an inner protection system against short-circuit, under-voltage of module's power supply, and over-temperature fault in module.

Up to now all the aforementioned above designed protection systems have worked several times and prepared a safe operation condition for the inverter against severe short-circuit or over-current faults.

4.2 Overvoltage

Transient overvoltage due to switching and leakage inductance is the common source of overvoltage in power electronics converter. Snubber circuits and transient voltage suppressors like Break Over Diode (BOD), Metal Oxide Varistor (MOV) and Transient Voltage Suppressor (TVS) diodes are the remarkable protection methods. In present studied application, snubber circuits (*C* type) and MOV protection methods are used to protect power inverter modules against any probable transient over-voltages. Up to know this protection system has worked at least two times, both when a short circuit fault has been happened incidentally by the output local AC load and as a result a transient overvoltage due to abrupt change in output current and DC-link leakage inductance is occurred.

Steady-state overvoltage may occur at input DC-link or output AC inverter's terminals. In this case, it is recommended to trip the power electronics converter and inform operator to remove the fault. To do this a Programmable Logic Controller (PLC) or microcontroller such as DSP can monitor the system and inform operator in the case of overvoltage fault condition.

DC over/under voltage protection monitors DC-link voltage and turn off IGBT switches consequential a fault. Since electronic systems, micro controller, IGBT drivers and so on are often supplied through dc link; it is necessary to consider dc-link under voltage protection.

A summary of protection system is shown in Figure 8. Almost all protections are done in DSP; backup hardware protection is also included to ensure the highest protection level. As the most effective protection strategy, all switches are turned off after fault detection by protection system.
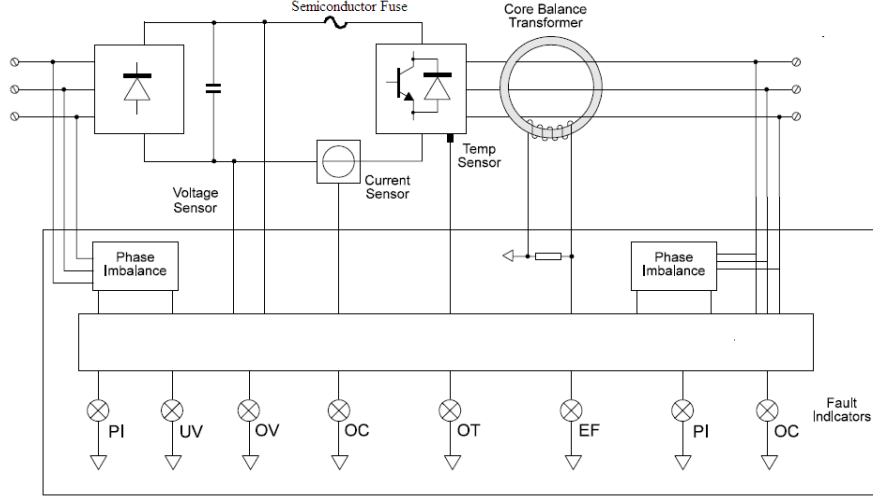
Figure 8: Protection system.

5 LCL Filter Design

Figure 2 shows the system topology of 85 kVA grid-tied AC/DC/AC converter for the microturbine-based power generation system. In this converter an *LCL* filter is used to connect the inverter output with the grid.

The *LCL* filter generally is used to decrease the switching ripple. In fact, compared with the *L* filter, an *LCL* filter with only a small increase in filter hardware could decrease the switching ripple adequately, and its components could be characterized as the following:

$$Z_I = R_I + L_I s \tag{2}$$

$$Z_G = (R_G + R_S) + (L_G + L_S)s \tag{3}$$

$$Z_O = R_D + \frac{1}{C_F s} \tag{4}$$

Here, L_I and R_I are the inverter-side inductance and its Equivalent Series Resistor (ESR), respectively; L_G and R_G are the grid-side inductance and its ESR; L_S and R_S are the equivalent series inductance and resistor (impedance) of the source. C_F is the capacitance of the *LCL* filter which is in series with R_D, the damping resistor of the *LCL* filter.

Three transfer functions related to the *LCL* filter that are useful to design filter's different parameters and also adjust inverter's current controller, are given as

$$G_{V_i I_1}(s) = \frac{I_1(s)}{V_i(s)} = \frac{Z_o + Z_g}{Z_i Z_g + Z_g Z_o + Z_o Z_i} \tag{5}$$

$$G_{V_i I_2}(s) = \frac{I_2(s)}{V_i(s)} = \frac{Z_o}{Z_i Z_g + Z_g Z_o + Z_o Z_i} \tag{6}$$

$$G_{I_1 I_2}(s) = \frac{I_2(s)}{I_1(s)} = \frac{G_{V_i I_2}(s)}{G_{V_i I_1}(s)} = \frac{Z_o}{Z_o + Z_g} \qquad (7)$$

Here, $I_1(s)$ and $I_2(s)$ are the inverter output current and the grid-side current, and $V_i(s)$ is the voltage generated by the inverter at its terminals.

The following design considerations are taken into account to determine the *LCL* filter parameters:

1. The selection of the ripple current is a trade-off among inductor L_I size, IGBT switching and conduction losses, and inductor coil and core losses. The smaller the ripple current, the lower the IGBT switching and conduction losses, but the larger the inductor, resulting in larger coil and core losses. Typically, the ripple current can be chosen as 15%-35% of rated current. For this case, the ripple current is selected as 33.5% of the rated current. The maximum current ripple can be derived as in (8) [23]:

$$\Delta i_{L1,max} = \frac{1}{8} \cdot \frac{V_{dc}}{L_1 . f_{SW}} = 33.5\% . i_{rated} \qquad (8)$$

2. The selection of the capacitor is a trade-off between reactive power in C_F and L_I inductance. The more capacitance, the more reactive power flowing into the capacitor, and the more current demand from the L_I and the switches. As a result, the efficiency will be lower. The capacitance cannot be too small either. Otherwise, the inductance will be large in order to meet the attenuation requirements. The larger inductance L_I resulted from smaller capacitance leads to higher voltage drop across the inductor L_I. In this design, the reactive power is chosen as 15% of the rated power [24].

$$C_F = 15\% . \frac{P_{rated}}{2\pi f_{Line} . V_{LL}^2} \qquad (9)$$

3. The resonance frequency should be included in a range between ten times the line frequency and one half of the switching frequency in order not to create resonance problems in the lower and higher parts of the harmonic spectrum. The passive resistors should be chosen as a compromise between the necessary damping and the losses in the system [25].

$$f_{res} \cong \frac{1}{2\pi} \sqrt{\frac{L_i + L_g}{L_i L_g C_F}} \qquad (10)$$

4. Passive damping must be sufficient to avoid oscillation, but losses cannot be so high as to reduce efficiency [26].

$$R_D = 50\% \times \frac{1}{2\pi f_{res} . C_F} \qquad (11)$$

Table 1 shows the system parameters.

Figure 9 shows the magnitude plot of the *LCL* filter transfer functions. As it could be seen from this figure the filter in the low-frequency range (below resonant frequency) can be approximated as the sum of the overall inductance ($L_I + L_G + L_S$); and in the high frequency range, as the inverter side inductor alone (L_I). It is assumed that at high frequencies, the capacitor acts as a short circuit.
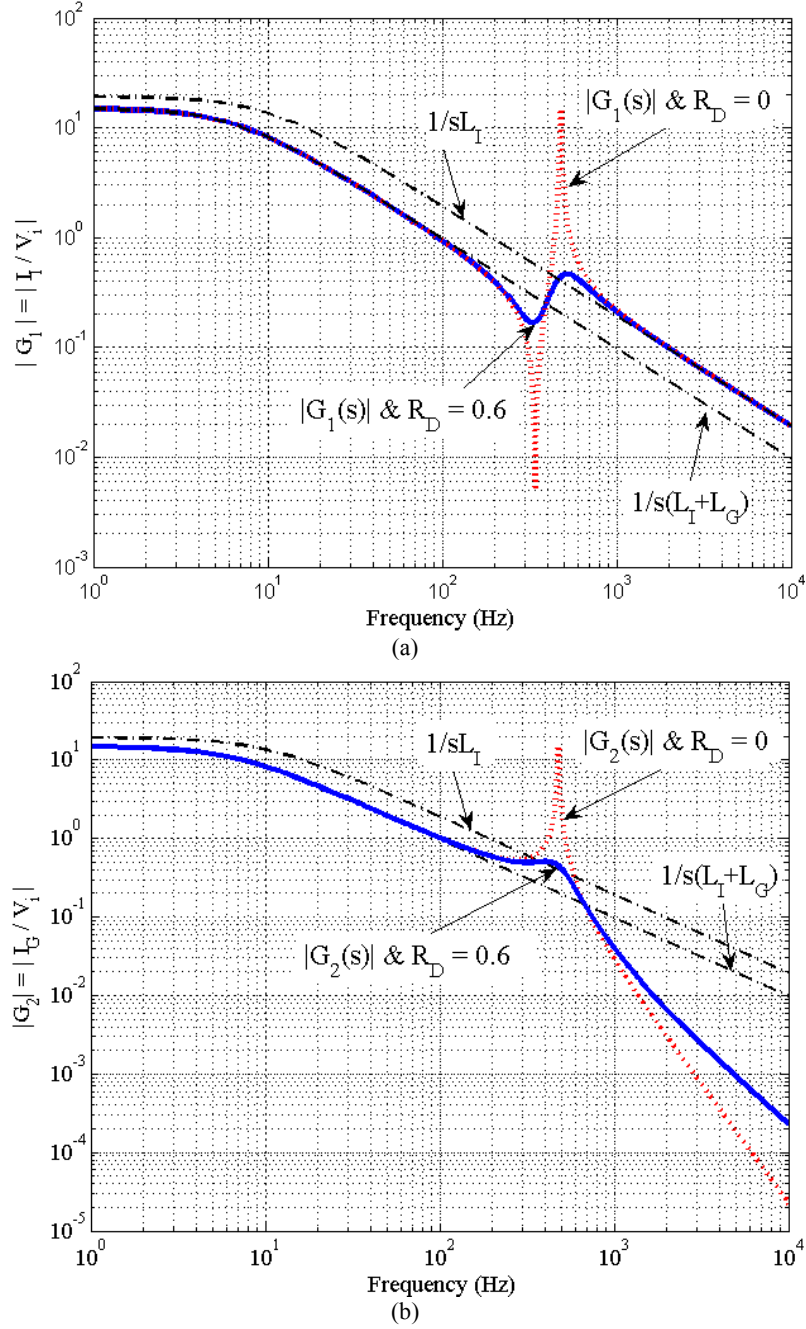
(a)

(b)

Figure 9: *LCL* filter forward admittance transfer function magnitude plots versus frequency; (a) forward self-admittance transfer function *G₁(s)*; (b) forward trans-admittance *G₂(s)*.

6 Proportional Resonance Controller Implementation

6.1 PR transfer functions

Generalised AC integrators are expressed as:

$$\frac{Y(s)}{E(s)} = \frac{2K_i s}{s^2 + \omega^2} \tag{12}$$

$$\frac{Y(s)}{E(s)} = \frac{2K_i\omega_c s}{s^2 + 2\omega_c s + \omega^2} \tag{13}$$

Equation (12), when grouped with a proportional term K_p, gives the ideal PR controller with an infinite gain at the AC frequency of ω, and no phase shift and gain at other frequencies. For K_p, it is tuned in the same way as for a PI controller, and it basically determines the dynamics of the system in terms of bandwidth, phase and gain margin.

To avoid stability problems associated with an infinite gain, (13) can be used instead of (12) to give a non-ideal PR controller and its gain is now finite, but still relatively high for enforcing small steady-state error. Another feature of (13) is that, unlike (12), its bandwidth can be widened by setting ω_c appropriately, which can be helpful for reducing sensitivity towards (for example) slight frequency variation in a typical utility grid (for (12), K_i can be tuned for shifting the magnitude response vertically, but this does not give rise to a significant variation in bandwidth).

Besides single frequency compensation, selective harmonic compensation can also be achieved by cascading several resonant blocks tuned to resonate at the desired low-order harmonic frequencies to be compensated for. As an example, the transfer functions of an ideal and a non-ideal harmonic compensator (HC) designed to compensate for the 3rd, 5th and 7th harmonics (as they are the most prominent harmonics in a typical current spectrum) are given as:

$$G_h(s) = \sum_{h=3,5,7} \frac{2K_{ih}\omega_c s}{s^2 + 2\omega_c s + (h\omega)^2} \tag{14}$$

where h is the harmonic order to be compensated for and K_{ih} represents the individual resonant gain, which must be tuned relatively high (but within stability limit) for minimising the steady-state error. An interesting feature of the HC is that it does not affect the dynamics of the fundamental PR controller, as it compensates only for frequencies that are very close to the selected resonant frequencies. It should be noted that as, ω_c gets smaller, $G_h(s)$ becomes more selective (narrower resonant peaks). However, using a smaller ω_c will make the filter more sensitive to frequency variations, lead to a slower transient response and make the filter implementation on a low-cost 16-bit DSP more difficult owing to coefficient quantisation and round-off errors. In practice, ω_c values of 5–15 rad/s have been found to provide a good compromise [10].

6.2 Implementation of resonant controllers

The resonant transfer functions in (13) can be implemented using a digital signal processor (DSP), such as TMS320F2812 or TMS320F28335, Texas Instrument 32-bit Fixed-Point and Floating-Point DSPs, respectively. Because of this, two methods of digitising the controllers are presented in detail.

6.2.1 Shift-operator digital implementation

The most commonly used digitisation technique is the pre-warped bilinear (Tustin) transform [18], given by:

$$s = \frac{\omega_{pw}}{\tan(\omega_{pw}T_s/2)} \frac{z-1}{z+1} = K_{Tu}\frac{z-1}{z+1} \tag{15}$$

where ω_{pw} is the pre-warped frequency, T_s is the sampling period and z is the forward shift operator. Equation (15) can then be substituted into (13) for obtaining the z-domain discrete transfer function given in (16), from which the difference equation needed for DSP implementation is derived and expressed in (17) (where n represents the point of sampling):

$$\frac{Y(z)}{E(z)} = \frac{\beta_1 z^{-1} - \beta_2 z^{-2}}{\alpha_0 - \alpha_1 z^{-1} + \alpha_2 Z^{-2}}$$

$$\beta_1 = \beta_2 = 2K_i K_T \omega_c$$

$$\alpha_0 = K_{Tu}^2 + 2K_{Tu}\omega_c + \omega^2 \tag{16}$$

$$\alpha_1 = 2K_{Tu}^2 - 2\omega^2$$

$$\alpha_2 = \begin{cases} K_{Tu}^2 + 2K_{Tu}\omega_c + \omega^2 \\ K_{Tu}^2 + 2K_{Tu}\omega_c + (h\omega)^2 \quad for \quad h = 3,5,7 \end{cases}$$

$$y(n) = \frac{1}{\alpha_0}\{\beta_1[e(n-1) - e(n-2)] + \alpha_1 y(n-1) \tag{17}$$
$$- \alpha_2 y(n-2)\}$$

Equations (16) and (17) can similarly be used for implementing the HC compensator after the desired harmonic order h is substituted. The resulting difference equation can conveniently be programmed into a floating-point DSP, but when a fixed-point DSP is used instead, coefficients of (17) have to be normalised by multiplying them with the maximum integer value of the chosen word length [10, 19]. This multiplication is needed for minimizing the extent of coefficient quantisation error, and the choice of word length is solely dictated by the size of error that can be tolerated (large coefficient quantisation error should be avoided since it can change the frequency characteristics of a resonant peak, and even render it 'open-loop' unstable). Unfortunately, no standard method of choosing this word length is available and, as discussed in [10, 19], the appropriate word length is usually determined experimentally with the aim of achieving the best tradeoff between execution speed and accuracy.

6.2.2 δ-operator digital implementation

Generally, when the shift-operator resonant implementation given in (16) and (17) is programmed into a fixed-point DSP, some performance degradations can usually be observed and are caused mainly by round-off errors associated with the use of integer variables on the fixed-point DSP (so-called finite word length effect). 16-bit fixed-point implementation always has finite word length effects, but the problem is particularly pronounced at a fast sampling rate and for sharply tuned filters such as the resonant function used for PR control. Specifically, the round-off errors cause the voltage or current wave shape to change slightly from cycle to cycle, resulting in significant fluctuations in its RMS value, as proven in [10].

To improve the resonant precision, the use of delta operator δ in place of the conventional shift operator has been investigated. The delta operator has recently gained importance in fast digital control owing to its superior finite word length performance [19–22], and it can be defined in terms of the shift operator z as:

$$\delta^{-1} = \frac{\Delta z^{-1}}{1 - z^{-1}} \tag{18}$$

Essentially, delta-operator resonant implementation involves converting a second-order section in z into a corresponding second-order Section in δ, as follows:

$$Q(z) = \frac{\alpha_0 + \alpha_1 z^{-1} + \alpha_2 z^{-2}}{1 + \beta_1 z^{-1} + \beta_2 z^{-2}}$$

$$\Rightarrow Q(\delta) = \frac{a_0 + a_1 \delta^{-1} + a_2 \delta^{-2}}{1 + b_1 \delta^{-1} + b_2 \delta^{-2}} \tag{19}$$

where $a_0 = \alpha_0$, $a_1 = (2\beta_0 + \alpha_1)/\Delta$, $a_2 = (\alpha_0 + \alpha_1 + \alpha_2)/\Delta^2$, $b_0 = 1$, $b_1 = (2 + \beta_1)/\Delta$, $b_2 = (1 + \beta_1 + \beta_2)/\Delta^2$, and Δ is a positive constant less than unity, which is carefully chosen to select the appropriate ranges for the β and α coefficients, and to minimize o the r internal variable truncation noise [22]. Equation (19)

is then implemented using the transposed direct form II (DFIIt) structure shown in Fig. 10. The DFIIt structure is chosen out of the many filter structures available because it has the best round-off noise performance for delta-operator-based filters [22]. From Fig. 10, the difference equations to be coded for the DSP can be written, in processing order, as:

$$r_4(n) = \Delta r_3(n-1) + r_4(n-1)$$
$$r_2(n) = \Delta r_1(n-1) + r_2(n-1)$$
$$y(n) = a_0 x(n) + r_4(n) \qquad\qquad (20)$$
$$r_3(n) = a_1 x(n) - b_1 y(n) + r_2(n)$$
$$r_5(n) = a_2 x(n) - b_2 y(n)$$

Note that the first two equations in (20) for $r_4(n)$ and $r_2(n)$ are obtained from the definition of the delta operator given in (18). In addition, similar to (17), the coefficients in (20) will initially be floating-point numbers and must be normalised by multiplying them with the maximum integer value of the chosen word length for faster and accurate execution in a fixed-point DSP. This required word length and the constant Δ together represent two degrees of design freedom that can be used for optimising the round-off performance against coefficient quantisation and potential overflows, often through experimental testing.
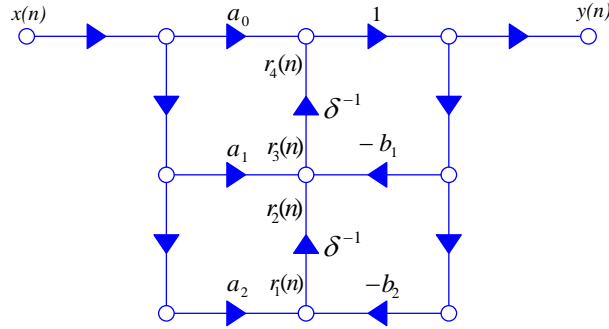

Figure 10: Direct form II transpose (DFIIt) structure for second-order digital filter

7 Experimental Results

The constructed inverter is tested under different load and grid scenarios. A photograph of constructed setup is shown in Figure 11. First, islanding operation of inverter is evaluated. Figure 12 shows the experimental results of this test. Figures 12 (a–b) and 12 (c–d) are demonstrated the experimental results of islanding operation when the reference voltage is changed between two different constant values. Experimental results shows the inverter have a good performance in the stand-alone mode of operation.
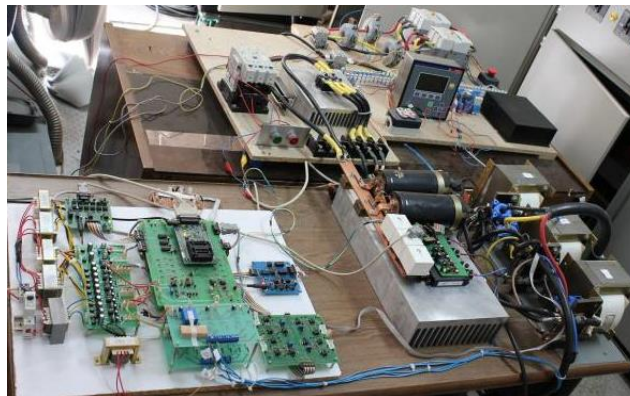

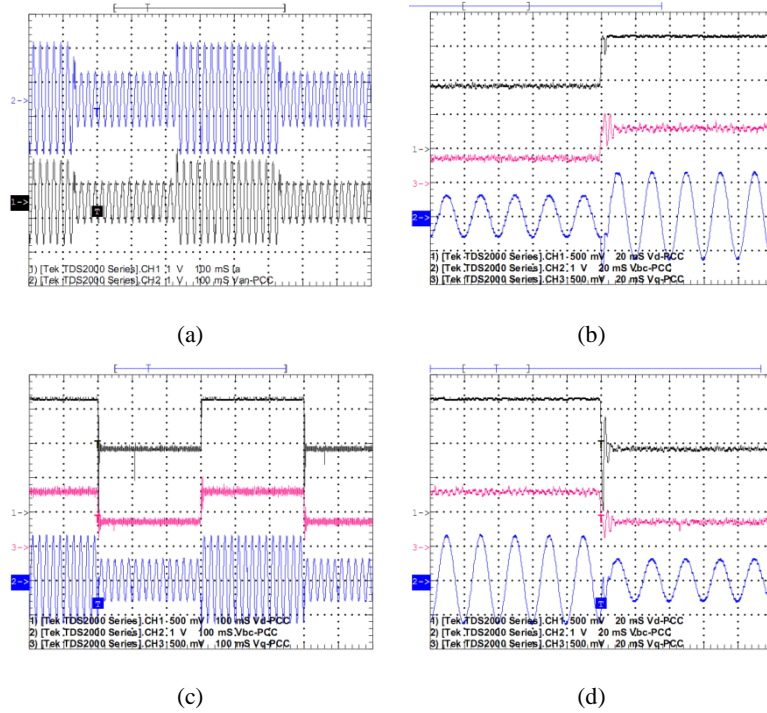Figure 11: Photograph of constructed DC/AC converter.

(a)   (b)

(c)   (d)

Figure 12: Experimental results when the inverter works in stand-alone mode: waveforms from top to bottom are (a) $V_{ab\text{-}PCC}$ & i_a; (b, c, and d) $V_{d\text{-}PCC}$ & $V_{q\text{-}PCC}$ & $V_{ab\text{-}PCC}$.

Second test scenario is the seamless transfer process between two control modes. Figs 13(a) shows first step of seamless transfer process described in section 3.3.1 In these Figure the bottom waveform is the phase difference between voltages at the PCC and the grid, named $\Delta\theta_{PG}$. Figure 13(b) demonstrates one step of seamless transfer process. The fourth waveform, *CSG*, shows a criterion variable that DSP evaluates the seamless transfer before sending a closing command to the relay *K*. Also, the third waveform shows the feedback signals that relay *K* send back to the DSP and shows the present statues of relay. Figures 13(c) and (d) show waveforms of the voltage and the current of inverter and grid when transferring between different modes are under processing.
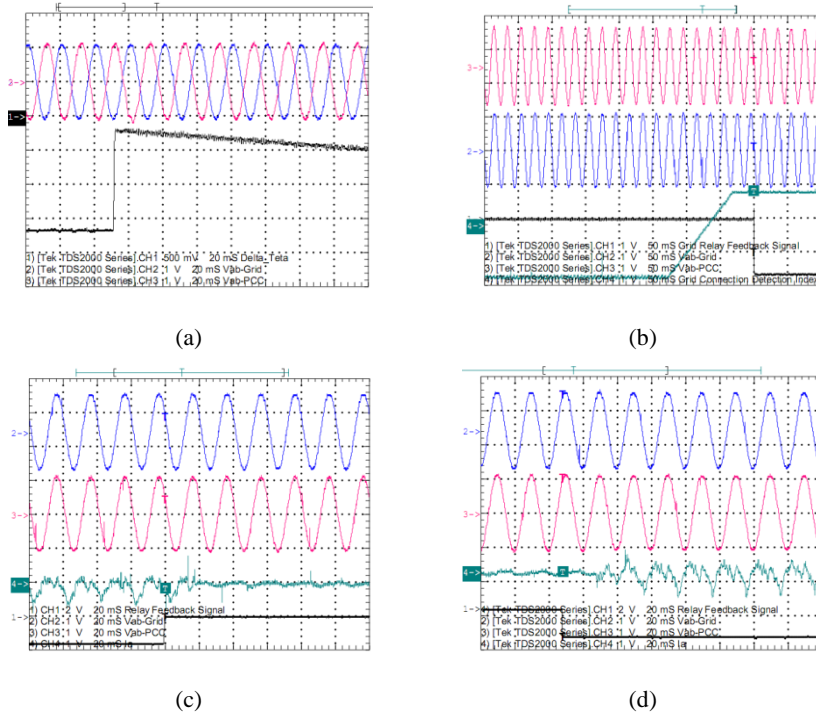
(a)   (b)

(c)   (d)

Figure 13: Experimental results when the inverter works in seamless transfer process:
waveforms from top to bottom are (a) V_{ab-PCC}, $V_{ab-grid}$ & $\Delta\theta_{PG}$; (b) $V_{ab-grid}$ & V_{ab-PCC} & SFR
& CSG; (c, and d) $V_{ab-grid}$ & V_{ab-PCC} & i_a & SFR.

   Experimental results related to the grid-connected control mode are depicted in Figure 14. The
grid voltage and inverter current waveforms are shown in Figures 14(a) and (b) when the reference
active and reactive power is changed from zero (in Fig, 14(a)) to 5 kW & 2 kVAr (in Fig 14(b)).
The output current of inverter, as shown in Figure 14(b), is highly distorted. The main reason for
this current distortion is the grid voltage that has 3% of 5th harmonic and 1.5% of unbalanced
voltage. Figure 14(c) shows the inverter related voltage and current waveforms under an over-
current fault condition. In this test two voltage phases in grid side are replaced and then a
command of connecting to the grid has been sent to the DSP controller. As shown in the Figure
14(c), the software protection system is acted immediately and sent opening command to the relay
K (fourth waveform, SDR) but electromechanical relay K needs 45 ms time to be opened. During
this time, a set of current is flown from grid toward the filter capacitance bank.
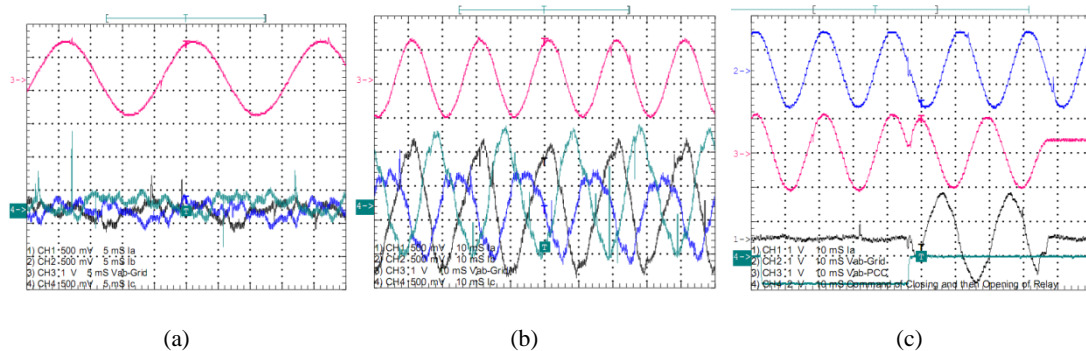
(a)   (b)   (c)

Figure 14: Experimental results when the inverter works in grid-connected mode: waveforms from top to bottom are (a, and b) $V_{ab\text{-}grid}$ & i_a, i_b, i_c; (c) $V_{ab\text{-}grid}$ & $V_{ab\text{-}PCC}$ & i_a & SDR.

8   Conclusion

Inverter is an important part of a microturbine-based distribution generation system. In this paper, a DSP-based digital controller in order to control a three-phase inverter in stand-alone and grid-connected modes is studied. The three-phase inverter, in fact, is a three-leg power converter which is switched in 2 kHz frequency by the controller with a sinusoidal PWM pattern. An 85 kVA three-phase inverter setup is developed and tested under different source and load scenarios. Experimental results prove the effectiveness and appropriate operation of designed controller. Based on experimental results in stand-alone control mode, output voltages are sinusoidal and balanced only with a low distortion level (voltage THD is less than 3%). In grid-connected control mode, distortion on grid voltage results a distorted inverter output current. To compensate this distortion, a harmonics suppression control block must be added to the inverter controller. The experimental results show that seamless transfer between two modes has been achieved well, but because of polluted grid voltage, waveform quality of the grid current is not good.

References

[1] A. Hasanzadeh, , C. Edrington, N. Stroupe , and T. Bevis, "Real-Time Emulation of A High-Speed Microturbine Permanent-Magnet Synchronous Generator Using Multiplatform Hardware-In-The-Loop Realization," Industrial Electronics, IEEE Transaction on, vol. 61, no. 6, pp. 3109-3118, June 2014.

[2] H. Karegar, and, A. Shabani, "Effects of Inverter Modulation Index on the Stability of Grid Connected Micro-Turbines," in Power and Energy Conference, 2008. PECon 2008. IEEE 2nd International, Dec 2008, pp. 1623-1627.

[3] Z. Ye, T. Wang, G. Sinha, and R. Zhang, "E_ciency comparison for microturbine power conditioning systems," in Power Electronics Specialist Conference, 2003. PESC '03. 2003 IEEE 34th Annual, vol. 4, June 2003, pp. 1551-1556 vol.4.

[4] M. S. Laili, Z. N. Zakaria, N. Halim, and P. Ibrahim, "Modelling and simulation of microturbine for a distribution system network with hybrid _lter," in Power Engineering and Optimization Conference (PEDCO) Melaka, Malaysia, 2012 IEEE International, June 2012, pp. 204-208.

[5] L. Wang and G.-Z. Zheng, "Analysis of a microturbine generator system connected to a distribution system through power-electronics converters," Sustainable Energy, IEEE Transactions on, vol. 2, no. 2, pp. 159-166, April 2011.

[6] M. Ranjbar, S. Mohaghegh, M. Salehifar, H. Ebrahimirad, and A. Ghaleh, "Power electronic interface in a 70 kw microturbine-based distributed generation," in Power Electronics, Drive Systems and Technologies Conference (PEDSTC), 2011 2nd, Feb 2011, pp. 111-116.

[7] S. Nayak and D. Gaonkar, "Modeling and performance analysis of microturbine generation system in grid connected/islanding mode," in Power Electronics, Drives and Energy Systems (PEDES), 2012 IEEE International Conference on, Dec 2012, pp. 1-6

[8] F.-S. Pai and S.-J. Huang, \Design and operation of power converter for microturbine powered distributed generator with capacity expansion capability," Energy Conversion, IEEE Transactions on, vol. 23, no. 1, pp. 110{118, March 2008.

[9] Y.-R. Mohamed, "Mitigation of dynamic, unbalanced, and harmonic voltage disturbances using grid-connected inverters with lcl _lter," Industrial Electronics, IEEE Transactions on, vol. 58, no. 9, pp. 3914-3924, Sept 2011.

[10] M. Ranjbar, H. Ebrahimirad, S. Mohaghegh, and A. Ghaleh, "Seamless transfer of three-phase grid-interactive microturbine inverter between grid-connected and stand-alone modes," in Electrical Engineering (ICEE), 2011 19th Iranian Conference on, pp. 1-1, May 2011.

[11] T.-V. Tran, T.-W. Chun, H.-H. Lee, H.-G. Kim, and E.-C. Nho, "Pll-based seamless transfer control between grid- connected and islanding modes in grid-connected inverters," Power Electronics, IEEE Transactions on, vol. PP, no. 99, pp. 1-1, 2013.

[12] D. Ochs and B. Mirafzal, "A method of seamless transitions between grid-tied and stand-alone modes of operation for utility-interactive three-phase inverters," Industry Applications, IEEE Transactions on, vol. PP, no. 99, pp. 1-1, 2013.

[13] F. Gonzalez-Espin, G. Garcera, I. Patrao, and E. Figueres, "An adaptive control system for three-phase photovoltaic inverters working in a polluted and variable frequency electric grid," Power Electronics, IEEE Transactions on, vol. 27, no. 10, pp. 4248-4261, Oct 2012.

[14] M. Castilla, J. Miret, A. Camacho, J. Matas, and L. de Vicuna, "Reduction of current harmonic distortion in three-phase grid-connected photovoltaic inverters via resonant current control," Industrial Electronics, IEEE Transactions on, vol. 60, no. 4, pp. 1464-1472, April 2013.

[15] Z. Liu, J. Liu, and Y. Zhao, "A uni_ed control strategy for three-phase inverter in distributed generation," Power Electronics, IEEE Transactions on, vol. 29, no. 3, pp. 1176-1191, March 2014.

[16] M. Castilla, J. Miret, A. Camacho, J. Garcia de Vicuna, and J. Matas Alcala, "Modeling and design of voltage support control schemes for three-phase inverters operating under unbalanced grid conditions," Power Electronics, IEEE Transactions on, vol. PP, no. 99, pp. 1-1, 2014.

[17] IEEE Draft Recommended Practice for Interconnecting Distributed Resources with Electric Power Systems Distribution Secondary Networks," IEEE P1547.6/D7.0, June 2010, pp.1-31. Sep 2010.

[18] M. Marwali and A. Keyhani, "Control of distributed generation systems-part i: Voltages and currents control," Power Electronics, IEEE Transactions on, vol. 19, no. 6, pp. 1541-1550, Nov 2004.

[19] R.-J. Wai, C.-Y. Lin, Y.-C. Huang, and Y.-R. Chang, "Design of high-performance stand-alone and grid-connected inverter for distributed generation applications," Industrial Electronics, IEEE Transactions on, vol. 60, no. 4, pp. 1542-1555, April 2013.

[20] R. Teodorescu and F. Blaabjerg, "Flexible control of small wind turbines with grid failure detection operating in stand-alone and grid-connected mode," Power Electronics, IEEE Transactions on, vol. 19, no. 5, pp. 1323-1332, Sep 2004.

[21] I. Gabe, V. Montagner, and H. Pinheiro, "Design and implementation of a robust current controller for VSI connected to the grid through an lcl filter," Power Electronics, IEEE Transactions on, vol. 24, no. 6, pp. 1444-1452, June 2009.

[22] X. Wang, X. Ruan, S. Liu, and C. Tse, "Full feedforward of grid voltage for grid-connected inverter with lcl _lter to suppress current distortion due to grid voltage harmonics," Power Electronics, IEEE Transactions on, vol. 25, no. 12, pp. 3119-3127, Dec 2010.

[23] T.C. Wang, Z. Ye, G. Sinha, X. Yuan, "Output Filter Design for a Grid-Interconnected Three-Phase Inverter," In: IEEE 34th Annual power Electronics Specialist Conference, 15-19 June 2003, pp.779-784, June 2003.

[24] M. Liserre, F. Blaabjerg, S. Hansen, "Design and Control of an LCL-Filter-Based Three-Phase Active Rectifier," In: IEEE Trans. Ind Appl 2005, vol. 41, no. 5, pp. 1281-1291, October 2005.

[25] A.A. Rockhill, M. Liserre, R. Teodorescu, P. Rodriguez, "Grid-Filter Design for a Multi megawatt-Medium-Voltage Voltage-Source Inverter," IEEE Trans Ind Electron 2011, vol. 58, no. 4, pp. 1205-1217, April 2011.

[26] M. Simoes, A. Reznik, , A. Al Durra, S.M Muyeen, "LCL Filter Design and Performance Analysis for Grid Interconnected Systems," IEEE Transactions on Industry Applications, vol 33. PP, no. 99, pp.1 , March 2014.